NUMERICAL PARAMETRIC STUDY OF COMPLEX LIQUID FLOW IN THREE-DIMENSIONAL IMPELLER AND IMPELLER-VOLUTE OF A CENTRIFUGAL PUMP

Massinissa Djerroud, Guyh Dituba Ngoma and Walid Ghie
University of Quebec in Abitibi-Témiscamingue, Department of Applied Sciences
445, Boulevard de l'Université, Rouyn-Noranda, Quebec, J9X 5E4, Canada

Keywords: Centrifugal Pump, Impeller, Volute, Navier-Stokes, Computational Fluid Dynamics, Modeling and Simulation.

Abstract: In this study, the effects that the blade width, the blade number, and the impeller diameter have on the steady state liquid flow in three-dimensional impeller, and combined impeller and volute were investigated. The continuity and Navier-Stokes equations with the k-ε turbulence model and the standard wall functions were used by mean of ANSYS-CFX code taking into account of the suction pressure variation as a function of the valve volume flow rate. The achieved results reveal that the selected key design parameters have an impact on the head, the brake horsepower and the overall efficiency of the centrifugal pump. To valid the developed approach, the results of numerical simulation were compared with the experimental results considering a special case of combined impeller and diffuser.

1 INTRODUCTION

Nowadays, centrifugal pumps are widely used in industrial and mining enterprises. One of the most important components of a centrifugal pump is the impeller (Peng, W. W., 2008). The performance characteristics related to the pump rely a great deal on the impeller. To achieve better performance for a centrifugal pump, design parameters such as the number of blades, blade angles, the blade width, the blade height, the impeller diameter and the volute radius must be accurately determined, due to the complex liquid flow through a centrifugal pump. This liquid flow is three-dimensional and turbulent. It is therefore important to be aware of the liquid flow's behavior when traveling through an impeller. This can be done by accounting for the volute in the planning, design, and optimization phases at conditions of design and off-design. Many studies have been carried out on the liquid flow through a centrifugal pump (Zhou, W. et al., 2003; Derakhshan, S., et al., 2008; Spence, R., et al., 2008; Amaral-Teixeira, J., et al., 2008; Cheah, K.W., 2007; Lee, T. S., et al., 2007; Wen-Guang, L., et al, 2002; LIU, H., et al., 2010; González, J., et al., 2007; Asuaje, M., et al., 2005; Kaupert, K, et al., 1999), where the effects of the number of impeller blades on the pump's performance were examined experimentally by Wen-Guang, L., et al, 2002 and Liu, H., et al., 2010. González, J., et al., 2007 had numerically investigated the dynamic effects due to the impeller-volute interaction within a centrifugal pump, whereas the effects of the volute on velocity and pressure fields were examined by Asuaje, M., et al., 2005 and Kaupert, K, et al., 1999. The analysis of previous works clearly demonstrated that research results obtained are specific to the centrifugal pump design parameter values and thus cannot be generalized. In this work therefore a numerical study was performed using a finite volume method according to the CFX code (Ansys inc., 2008) to gain further insight into the characteristics of the three-dimensional turbulent liquid flow through an impeller and a combined impeller and volute accounting for suction pressure variation as a function of the valve volume flow rate, while also considering various flow conditions and pump design parameters: blade width, blade number and impeller outer diameters.

2 GOVERNING EQUATIONS

The models selected for the liquid flow in an

Djerroud M., Dituba Ngoma G. and Ghie W..
NUMERICAL PARAMETRIC STUDY OF COMPLEX LIQUID FLOW IN THREE-DIMENSIONAL IMPELLER AND IMPELLER-VOLUTE OF A CENTRIFUGAL PUMP.
DOI: 10.5220/0003566800930102
In *Proceedings of 1st International Conference on Simulation and Modeling Methodologies, Technologies and Applications* (SIMULTECH-2011), pages 93-102
ISBN: 978-989-8425-78-2

impeller and a combined impeller and volute are depicted in Fig. 1, placing greater emphasis on the fluid domain.

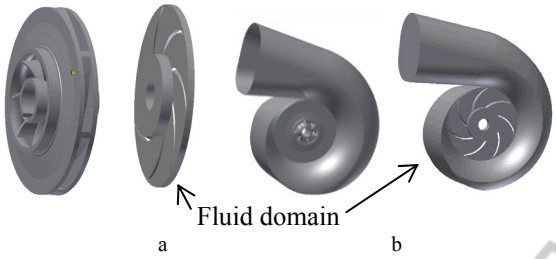

Figure 1: Models of a) impeller and b) impeller-volute.

In the governing equations for liquid flow in the centrifugal pump components, the following assumptions were made: (i) a steady state, three-dimensional and turbulence flow using the k-ε model; (ii) it was an incompressible liquid; (iii) it was a Newtonian liquid; and (iv) the liquid's thermophysical properties were constant with temperature.

To account for these assumptions, the theoretical analysis of the liquid flow in an impeller, and a combined impeller and volute, was based on the continuity and Navier-Stokes equations (Ansys inc, 2008). For the three-dimensional liquid flow through the components of a centrifugal pump as shown in Fig. 1, the continuity equations are expressed by:

$$\nabla.\vec{U} = 0 , \tag{1}$$

and the Navier–Stokes equations are given by:

$$\rho\nabla.(\vec{U}\otimes\vec{U}) = -\nabla p + \mu_{eff}\nabla.(\nabla\vec{U} + (\nabla\vec{U})^{T}) + B \tag{2}$$

where $\vec{U} = \vec{U}(u(x,y,z), v(x,y,z), w(x,y,z))$ is the liquid flow velocity vector, p is the pressure, ρ is the density, μ_{eff} is the effective viscosity accounting for turbulence, ⊗ is a tensor product and B is the source term. More particularly, for flows in an impeller rotating at a constant speed ω, the source term can be written as follows:

$$B = -\rho\left(2\vec{\omega}x\vec{U} + \vec{\omega}x\left(\vec{\omega}x\vec{r}\right)\right) \tag{3}$$

where $\vec{r}$ is the location vector.
In addition, μ_{eff} is defined as:

$$\mu_{eff} = \mu + \mu_t \tag{4}$$

where μ is the dynamic viscosity and μ_t is the turbulence viscosity.

According to the k-ε turbulence model, μ_t is linked to turbulence kinetic energy κ and dissipation ε via the relationship:

$$\mu_t = C_\mu \rho k^2 \varepsilon^{-1} \tag{5}$$

where C_μ is a constant.
The values for κ and ε come directly from the differential transport equations for turbulence kinetic energy and turbulence dissipation rates:

$$\nabla.(\rho\vec{U}k) = \nabla.[(\mu + \frac{\mu_t}{\sigma_k})\nabla k] + p_k - \rho\varepsilon \tag{6}$$

$$\nabla.(\rho\vec{U}\varepsilon) = \nabla.[(\mu + \frac{\mu_t}{\sigma_\varepsilon})\nabla\varepsilon] + \frac{\varepsilon}{k}(C_{\varepsilon 1}p_k - C_{\varepsilon 2}\rho\varepsilon) \tag{7}$$

where $C_{\varepsilon 1}$, $C_{\varepsilon 2}$ and σ_ε are constants. p_k is the turbulence production due to viscous and buoyancy forces, which is modeled using:

$$p_k = \mu_t\nabla\vec{U}.(\nabla\vec{U} + \nabla\vec{U}^{T}) - \frac{2}{3}\nabla.U(3\mu_t\nabla.\vec{U} + \rho k) + p_{kb} \tag{8}$$

$$p_{kb} = -\frac{\mu_t}{\rho\sigma_\rho}g.\nabla\rho \tag{9}$$

where p_{kb} can be neglected for the k-ε turbulence model.

Moreover, for the modeling of flow near the wall, the logarithmic wall function is used to model the viscous sub-layer (Ansys Inc., 2008).

2.1 Impeller

Three velocity types are involved when considering the flow through a centrifugal pump impeller: the tangential velocity U = r ω, the relative velocity W, and the absolute velocity V. The last is expressed in vector format as follows:

$$\vec{V} = \vec{U} + \vec{W} \tag{10}$$

Fig. 2 shows the velocity triangles at the impeller inlet and outlet at the design conditions where the liquid enters and leaves the impeller at the blade angles β_{b1} and β_{b2}. The components of $\vec{V}$ and $\vec{W}$ in the direction of $\vec{U}$ are $V_{u,}$ (swirl velocity), and W_u, respectively, while those normal to $\vec{U}$ are V_r and W_r.

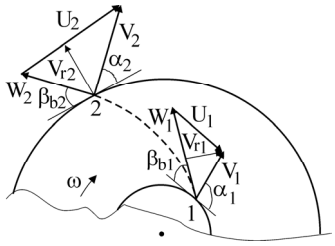

Figure 2: Velocity triangles.

Moreover, according to the Euler equation (Peng, W. W., 2008), the energy transfer per unit mass of flow for a centrifugal pump can be formulated as:

$$gH_i = U_2 V_{u2} - U_1 V_{u1} \tag{11}$$

where H_i is the ideal pump total head.
Neglecting the swirl velocity at the impeller inlet, Eq. 11 can be expressed as follows

$$gH_i = U_2 V_{u2} \tag{12}$$

When accounting for the hydraulic efficiency, η_h, the actual pump head rise is given by:

$$H = \eta_h H_i \tag{13}$$

Also, the hydraulic efficiency can be calculated using the following empirical formula (Peng, W. W., 2008):

$$\eta_h = 1 - 0.8\,(15859.03Q)^{-0.25} \tag{14}$$

where Q is the volume flow rate in m^3/s. It is given by $Q = V_r A$ with A as the flow passage area normal to the meridional direction.

Since in reality the flow through a centrifugal pump is turbulent and three dimensional, the actual relative flow direction at the impeller exit is different from that of the blade angle. As depicted in Fig. 3, the flow angle β_{f2} is always less than the blade angle β_{b2}. This can lead to secondary flows in the flow passage, from the pump inlet through to discharge (Peng, W. W., 2008).

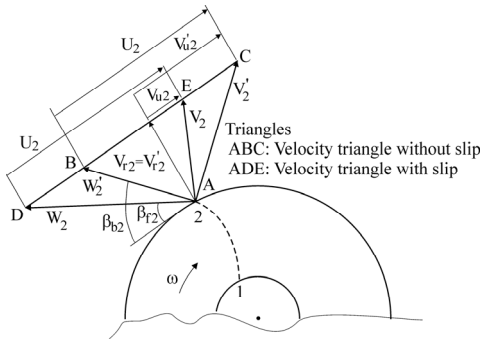

Figure 3: Flow angle and blade angle.

As such, the slip factor μ_s is used to take into account the difference between β_{b2} and β_{f2}, which is formulated as:

$$\mu_s = \frac{V_{u2}}{V'_{u2}} \tag{15}$$

where V_{u2} is the actual swirl flow velocity at the impeller exit and V'_{u2} is the ideal swirl flow velocity at the impeller exit.

In addition, the slip velocity is given by:

$$\Delta V_s = V'_{u2} - V_{u2} = W_{u2} - W'_{u2} \tag{16}$$

Taking into account the slip factor, Eq. 13 can be expressed as:

$$H = \eta_h \mu_s \left(\frac{U_2}{g}\right)\left(U_2 - \frac{Q}{A_2 \tan\beta_2}\right) \tag{17}$$

Moreover, to account for the leakage flow from the impeller, the volumetric efficiency is defined by:

$$\eta_v = \frac{Q + Q_L}{Q_L} \tag{18}$$

where Q_L is the leakage flow from the impeller exit back to the inlet through the clearance.

In addition, the pump's mechanical efficiency is formulated as follows:

$$\eta_m = \frac{P_{imp}}{P_s} \tag{19}$$

where P_s is the brake horsepower and P_{imp} the power delivered by the impeller to the fluid.

P_s is globally expressed by:

$$Ps = P_h + P_f + P_L + P_m + P_{df} = C\omega \tag{20}$$

where C is the pump shaft torque, P_h is the centrifugal pump horsepower. It is expressed as:

$$P_h = \rho Q g H \tag{21}$$

P_f is the loss power due to the friction, which is given by:

$$P_f = \rho Q g \left(H_i - H\right) \tag{22}$$

P_L is the loss power due to leakage, which is defined as:

$$P_L = \rho Q_L g H_i \tag{23}$$

P_m is the friction loss power in bearings and seals and P_{df} is the disk friction power due to impeller shrouds.

P_{imp} in Eq. 19 can be formulated as follows:

$$P_{imp} = P_s - P_m - P_{df} \quad (24)$$

Furthermore, Eq. 24 can be rewritten as :

$$P_{imp} = \rho(Q + Q_L)gH_i \quad (25)$$

Accounting for Eq. 24, Eq.19 can be expressed as:

$$\eta_m = \frac{P_s - P_m - P_{df}}{P_s} \quad (26)$$

Thus, the overall efficiency of a centrifugal pump can be formulated as:

$$\eta = \frac{P_h}{P_s} \quad (27)$$

Finally, the overall efficiency can also be formulated in terms of the other efficiencies as:

$$\eta = \eta_h \eta_v \eta_m \quad (28)$$

2.2 Volute Parameters

Fig. 4 shows the parameters of a volute defined by the radius of volute basic circle r_3, the radius of volute cut water circle r_v, the volute angle α_v, the volute cross-sectional area A_θ,which depends of the angle Θ, and the volute outlet cross-sectional area A_t (Peng, W. W., 2008).

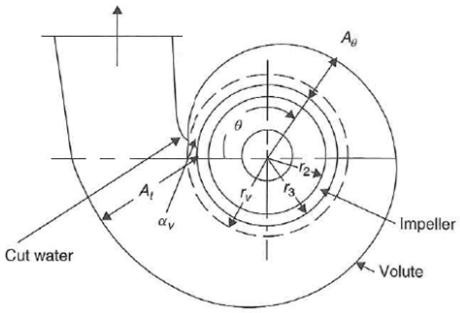

Figure 4: Impeller-volute.

The average flow velocity at the volute outlet is given by:

$$V_3 = K_3\sqrt{2gH} \quad (29)$$

where the volute velocity constant K_3 is an empirical parameter correlated with the specific speed, as shown in Fig. 5 along with other volute parameters such as the volute angle α_v and the volute basic circle diameter D_3.

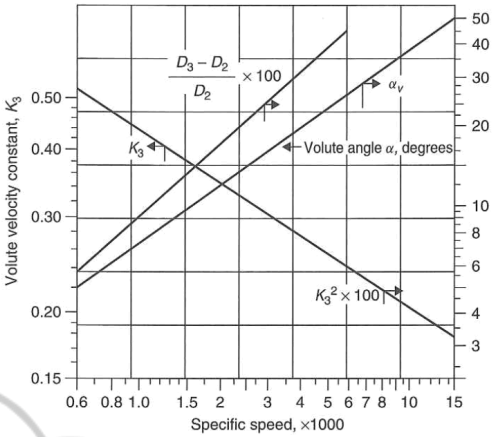

Figure 5: Volute velocity constant, volute angle and diameter of volute basic circle versus specific speed.

In addition, the volute cross-sectional area A_θ can be formulated as:

$$A_\theta = \frac{Q\theta}{2\pi CL} r_c \quad (30)$$

where r_c is the centroid radius of the volute cross-sectional area, L is the angular momentum of flow at the impeller outlet which can be expressed by $L = r_2 V_{u2}$. C≅ 0.95 to account for friction loss.

To solve Eqs. 1 and 2 numerically while accounting for the boundary conditions and the turbulence model κ-ε, the computational fluid dynamics ANSYS-CFX code, based on the finite volume method, was used to obtain the liquid flow velocity and the pressure distributions. In the cases examined involving the impeller, and combined impeller and volute, the boundary conditions were formulated as follows: the static pressure provided was given at the inlet, while the flow rate provided was specified at the outlet. The frozen rotor condition was used for the impeller-volute interface. A no-slip condition was set for the flow at the wall boundaries. Fig. 6 shows the inlet, outlet and interface domains for the selected centrifugal pump components.

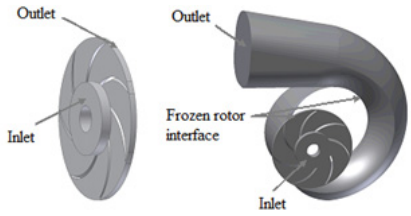

Figure 6: Domains of inlet, outlet and interface.

Furthermore, the ANSYS-CFX code comprises by geometry (DesignModeler), CFX-pre, CFX-solver

and CFX-post modules. According to the applied ANSYS-CFX code, Fig. 7 depicts the steps specifically used to obtain the numerical simulation results from the geometry models to the numerical models for the impeller, and the combined impeller and volute.

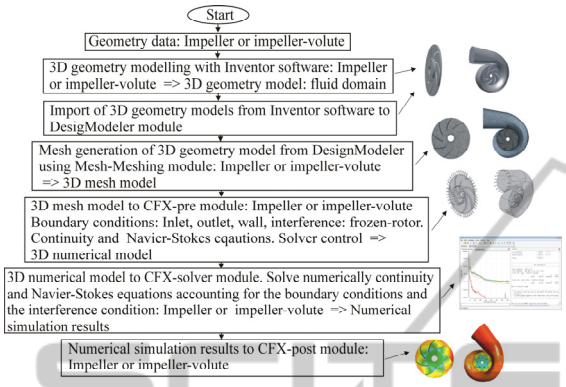

Figure 7: Steps from 3D geometry model to numerical simulation results.

3 RESULTS AND DISCUSSION

Water was used as the working liquid for all simulations run and for use in this study considered to have the following reference values: temperature of 25 °C for water, density of ρ = 997 kg/m³ and dynamic viscosity of $\mu = 8.899 \times 10^{-4}$ Pa s. The main data for the reference impeller and volute are given in Tabs. 1 (Technosub Inc) and 2 (Peng, W. W., 2008).

Table 1: Main data of the reference impeller.

Inlet diameter [mm]	145
Outlet diameter [mm]	320
Inlet blade angle [°]	11.69
Outlet blade angle [°]	28
Inlet blade width [mm]	12
Blade thickness [mm]	4
Number of blades	7
Rotating speed [rpm]	1800

Table 2: Main data of the reference volute.

Volute angle [°]	Volute radius [mm]	Volute angle [°]	Volute radius [mm]
0	165	225	278.96
45	183.79	270	302.76
90	207.58	315	326.55
135	231.38	360	350.35
180	255.17		

Accounting for the fact that the pump rotating speed was constant, the volume flow rate was controlled by a regulator valve, which had an influence on the pressure at the pump inlet, as shown in Fig. 8 (Technosub Inc.). This was accounted for in the numerical simulations performed.

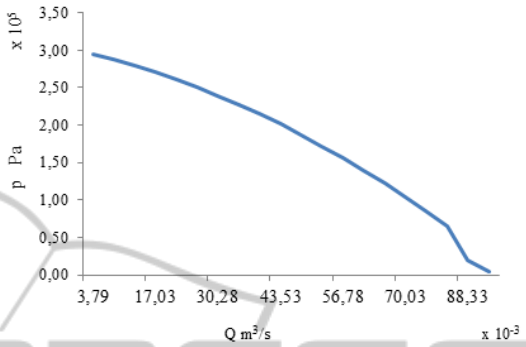

Figure 8: Pressure at the pump inlet versus valve volume flow rate regulation.

3.1 Case Studies

Three key design parameters of a centrifugal pump were selected for an examination of their effects mainly on the pump performance: impeller blade width without volute, impeller blade number with volute, impeller diameter with volute.

3.1.1 Effect of Impeller Blade Width

To investigate the effect that the impeller blade width has on the pump head, the pump brake horsepower and the pump overall efficiency, the blade widths of 4 mm, 10 mm and 15 mm were selected, while the other parameters were keep constant. Fig. 9 shows the pump head as a function of the volume flow rate, illustrating that the pump head decreases with increased blade width. This is due augmenting the liquid pressure drop with increasing blade width. Also, the required pump brake horsepower decreases when the blade width rises, as indicated in Fig. 10. The corresponding overall efficiency curves are shown in Fig. 11, illustrating that the blade width's impact on the overall efficiency is more pronounced in at high volume flow rates. In other words, the overall efficiencies for the three blade widths decrease rapidly to the right side of the best efficiency point (BEP) and the lowest overall efficiency is obtained when e = 15 mm.

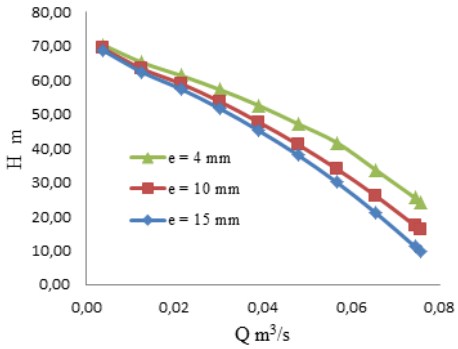

Figure 9: Pump head versus volume flow rate (blade width).

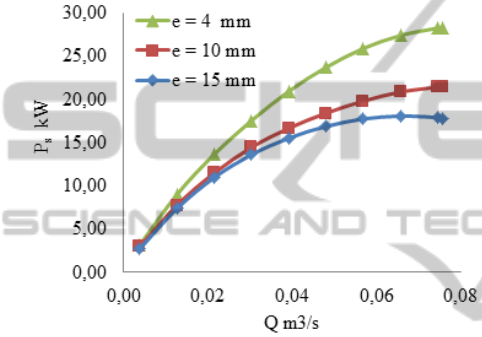

Figure 10: Pump brake horsepower versus Volume flow rate (blade width).

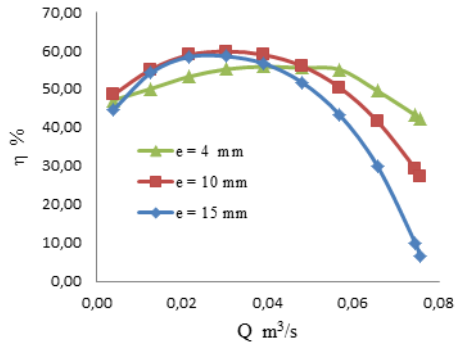

Figure 11: Overall efficiency versus volume flow rate (blade width).

In addition, Figs. 12 and 13 show the static pressure contour and the liquid flow velocity vector for Q = 0.065 m^3/s, illustrating that the static pressure difference between the impeller outlet and inlet decreases with increasing blade width, due to the increase in liquid flow velocity at the impeller outlet. The average liquid flow velocities at the impeller outlet are 15.92 m/s, 19.10 m/s and 20.57 m/s for e = 4 mm, e = 10 mm and e = 15 mm, respectively.

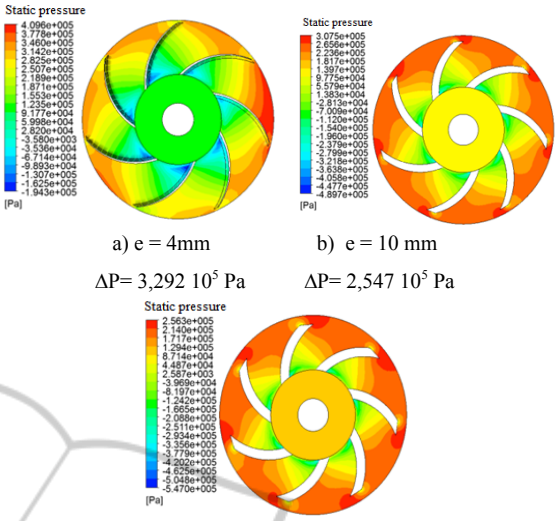

a) e = 4mm ΔP= 3,292 10^5 Pa

b) e = 10 mm ΔP= 2,547 10^5 Pa

c) e =15 mm ΔP= 2,056 10^5 Pa

Figure 12: Static pressure contour (blade width).

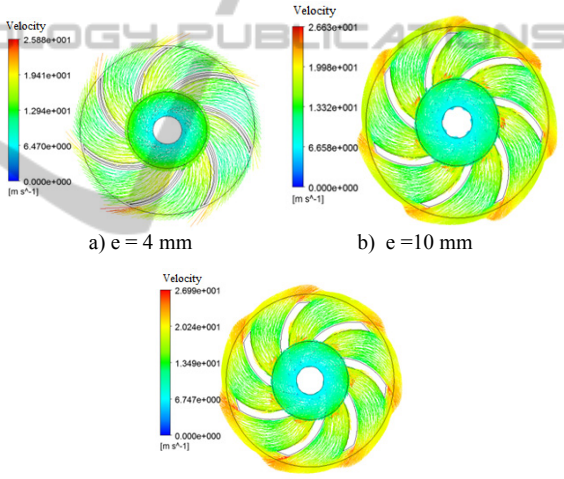

a) e = 4 mm

b) e =10 mm

c) e = 15mm

Figure 13: Liquid flow velocity vector (blade width).

3.1.2 Effect of Impeller Blade Number When Accounting for Volute

To analyze the effect of the impeller blade number on the pump head, the pump brake horsepower and the overall pump efficiency, three impellers whose blade number were 5, 7 and 9 were selected, while the other parameters were kept constant. Fig. 14 shows the pump head as a function of the volume flow rate, illustrating that the pump head increases with a greater blade number. This is explained by the decrease in the liquid pressure drop in the flow passage with an augmented impeller blade number, keeping the same total volume flow rate. Also, as

shown in Fig. 15, the pump brake horsepower increases relative with the augmented blade number. This is due to the increase in the request pump shaft torque, as the pump blade number also increases.

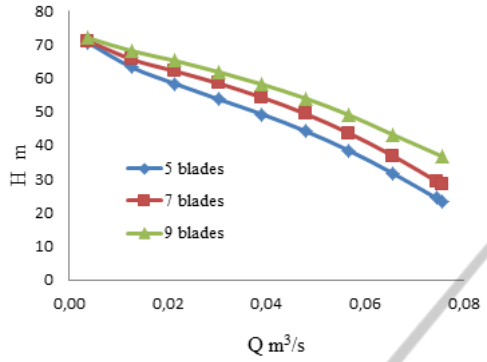

Figure 14: Pump head versus volume flow rate (parameter: impeller blade number).

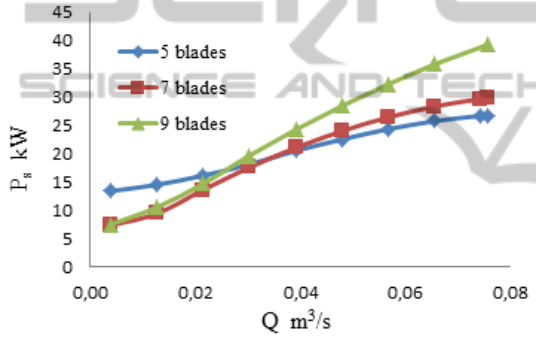

Figure 15: Brake horsepower versus volume flow rate (impeller blade number).

In addition, Fig. 16 shows the overall efficiency curves, showing that the impeller having 5 blades has the lowest overall efficiency.

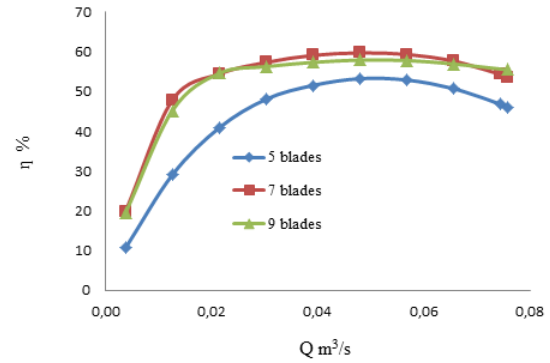

Figure 16: Overall efficient versus blade Number (blade number).

Moreover, Figs. 17 and 18 depict the corresponding static pressure contour and liquid flow velocity vector for Q = 0.065 m^3/s, respectively. These figures thus clearly show the increased static pressure difference between the volute outlet and the impeller inlet relative to the increasing blade number. This confirms the reduction in the liquid flow velocity at the impeller outlet relative to the greater blade number, as represented in Fig. 18 where the average liquid flow velocities at the impeller outlet were 16.06 m/s, 15.40 m/s et 12.53 m/s for 5 blades, 7 blades et 9 blades, respectively.

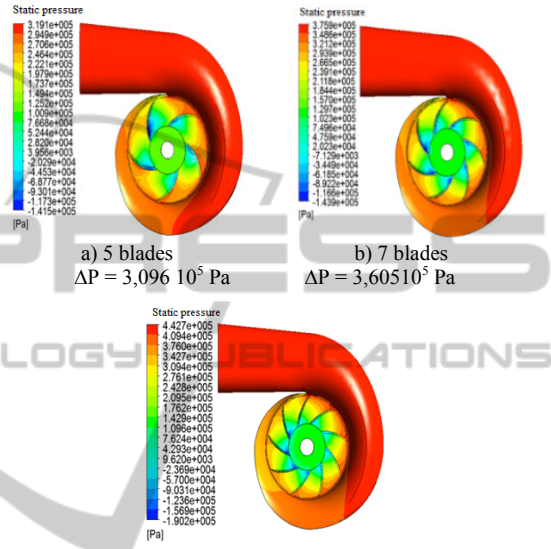

a) 5 blades
$\Delta P = 3{,}096\ 10^5$ Pa

b) 7 blades
$\Delta P = 3{,}60510^5$ Pa

c) 9 blades
$\Delta P = 4{,}223\ 10^5$ Pa

Figure 17: Static pressure contour (impeller blade number).

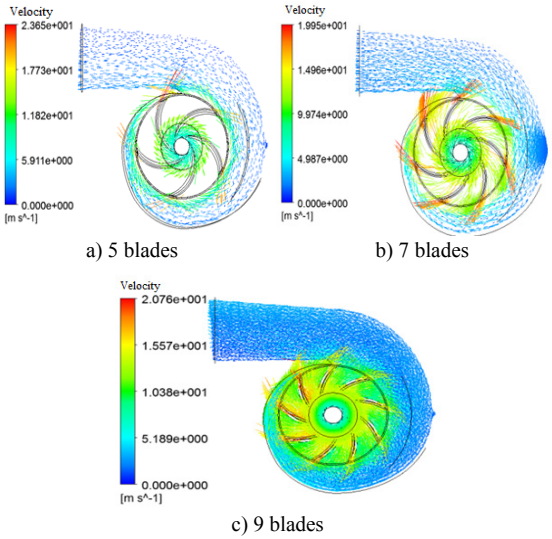

a) 5 blades

b) 7 blades

c) 9 blades

Figure 18: Vectors of liquid flow velocity contour (impeller blade number).

3.1.3 Effect of Impeller Diameter

The impeller outlet diameter values of 285 mm and 320 mm were selected to investigate their effects on pump performance when keeping the other parameters constant. Fig. 19 shows that the pump head increases with increasing impeller diameter, which can be explained by the fact that the liquid static pressure drop in impeller decreases with increasing impeller diameter. In other words, for a given volume flow rate, the pressure difference between the volute outlet and the impeller inlet is higher for an impeller with a greater diameter. In addition, Fig. 20 shows that the brake horsepower increases relative to the increasing impeller diameter, due to the requested augmented impeller shaft torque relative to the size of the impeller diameter.

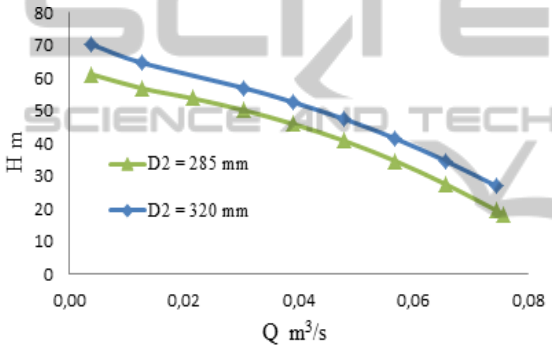

Figure 19: Pump head versus volume flow rate (impeller diameter).

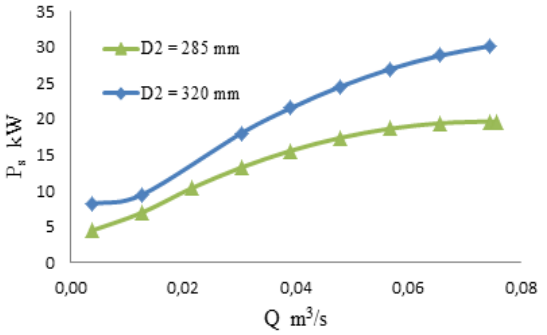

Figure 20: Brake horsepower versus volume flow rate (parameter: impeller diameter).

Moreover, the corresponding overall efficiency curves shown in Fig. 21 indicate that the impeller having a great diameter has better overall efficiency with volume flow rates greater than 0.02 m^3/s.

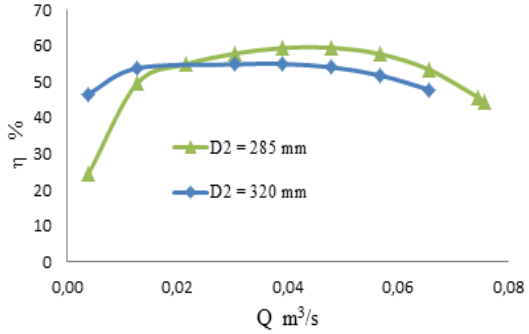

Figure 21: Overall efficiency versus volume flow rate (impeller diameter).

Additionally, Figs. 22 and 23 depict the static pressure contour and the liquid flow velocity vector. Fig. 22 thus clearly shows the correlation between the increase in static pressure difference between the volute outlet and the impeller inlet, and the increase in the impeller diameter. The average liquid flow velocities reached at the impeller outlet are 12.51 m/s and 15.40 m/s for D_2 = 285 mm and D_2 =320 mm, as shown in Fig. 23, respectively.

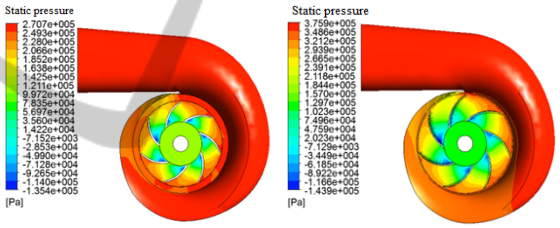

a) D = 285 mm
ΔP= 2,691 10^5 Pa

b) D=320mm
ΔP= 3,386 10^5 Pa

Figure 22: Static pressure contour (impeller diameter).

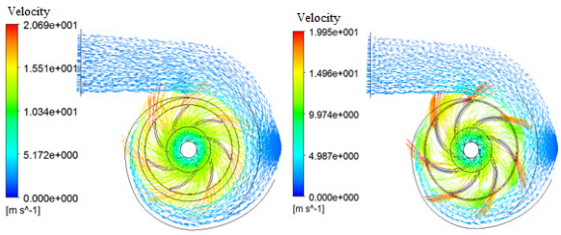

a) D = 285 mm

b) D=320mm

Figure 23: Vectors of liquid flow velocity (impeller diameter).

3.2 Model Comparison

Since the experimental results of the case of a combined impeller and diffuser were available from Technosub Inc., the developed numerical approach was validated transforming the case of a combined impeller and volute to a combined impeller and

diffuser. When taking into account of experimental boundary conditions for the numerical simulations run, Figs. 24-26 show the comparison between the experimental and the numerical results for the pump head, the brake horsepower and the overall efficiency. The discrepancies observed in these figures could be explained by the fact that lost mechanical power, power lost due to leakage and the pump casing were not taken into account in the numerical simulations carried out. The brake horsepower for experimental pump brake was therefore higher than the numerical brake horsepower obtained, as illustrated in Fig 25.

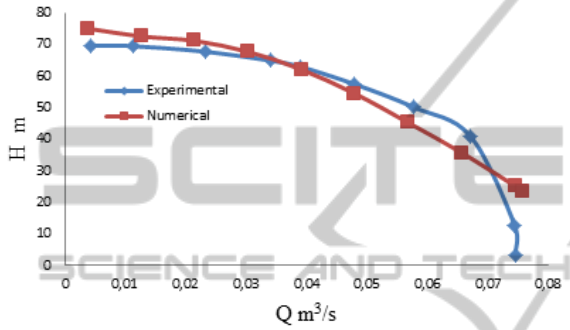

Figure 24: Pump head versus volume flow rate (numerical and experimental).

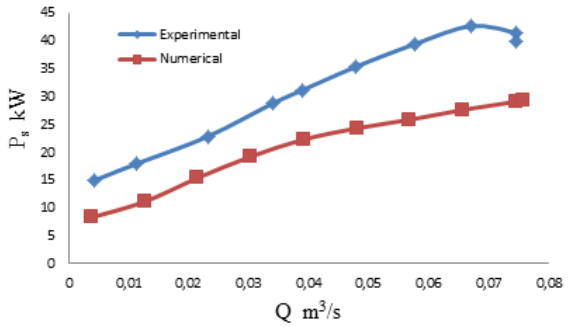

Figure 25: Brake horsepower versus volume flow rate (numerical and experimental).

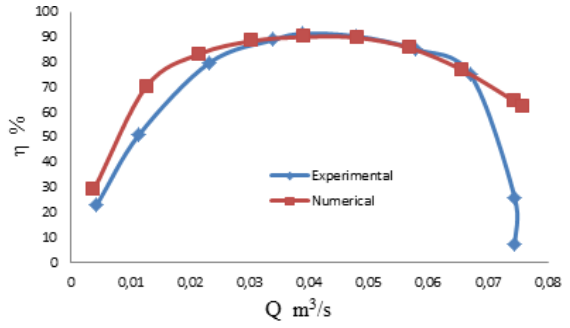

Figure 26: Overall efficiency versus volume flow rate (numerical and experimental).

4 CONCLUSIONS

In this research work, a steady state liquid flow in three-dimensional impeller, and combined impeller and volute of a centrifugal pump was numerically investigated using the ANSYS-CFX code. The obtained results demonstrate, among others, that the pump head and the brake horsepower increase with increasing impeller blade number, while they decrease with increasing impeller blade width. Also, the interaction between the impeller and the volute reveals that the decrease of the impeller outer diameter keeping the volute dimensions constant leads to the reduction of the pump head and the brake horsepower. The pump overall efficiency is also influenced by the selected parameter. A relatively good agreement was observed comparing the developed numerical approach with the experimental results for special case of the combined impeller and diffuser. Further research is planned to develop a generalized numerical approach for optimizing of combined impeller, diffuser and volute, accounting for experimental data from pump manufacturers.

ACKNOWLEDGEMENTS

The authors are grateful to the Foundation of University of Quebec in Abitibi-Témiscamingue (FUQAT) and the company Technosub inc.

REFERENCES

Peng, W. W., 2008, Fundamentals of turbomachinery, *John Wiley and Sons*. Hoboken, New Jersey.

Zhou, W., Zhao, Z., Lee, T. S. and Winoto, S. H., 2003, Investigation of Flow Through Centrifugal Pump Impellers Using Computational Fluid Dynamics. *Intern. J. of Rotating Machinery*, 9(1): 49–61.

Derakhshan, S., Nourbakhsh, A., 2008, Theoretical, numerical and experimental investigation of centrifugal pumps in reverse operation. *Exper. Thermal and Fluid Sc.* 32, 1620–1627.

Spence, R., Amaral-Teixeira, J., 2008, Investigation into pressure pulsations in a centrifugal pump using numerical methods supported by industrial tests. *Computers and Fluids* 37, 690–704.

Cheah, K. W., Lee, T. S., Winoto, S. H., and Zhao, Z. M., 2007, Numerical Flow Simulation in a Centrifugal Pump at Design and Off-Design Conditions. *Hindawi Publishing Corporation International Journal of Rotating Machinery*, Volume 2007, Article ID 83641, 8 pages.

Wen-Guang, L., Fa-Zhang, S. and Cong, X., 2002, Influence of the number of impeller blades on the performance of centrifugal oil pumps. *World Pumps*, Volume 2002, Issue 427, Pages 32-35.

Liu, H., Wang, Y., Yuan, S., Tan, M., and Wang, K., 2010, Effects of Blade Number on Characteristics of Centrifugal Pumps, *Chinese j. of mech. eng.*, Vol. 23, No. 6.

González, J., Fernández-Francos, J., Blanco, E. and Santolaria-Morros, C. 2002, Numerical simulation of the dynamic effects due to impeller-volute interaction in a centrifugal pump. *Transactions of the ASME, J. of Fluids Engineering*, vol. 124, no. 2, pp. 348–355.

Asuaje, M., Bakir, F., Kouidri, S., Kenyery, F., Rey, R., 2005, Numerical Modelization of the Flow in Centrifugal Pump: Volute Influence in Velocity and Pressure Fields. *Intern. J. of Rotating Machinery*: 3, 244–255.

Kaupert, K. A., Staubli, T. 1999, The Unsteady Pressure Field in a High Specific Speed Centrifugal Pump Impeller - Part I: Influence of the Volute. *Transactions of the ASME, J. of Fluids Engineering*, Vol. 121, 621-626.

Ansys inc., 2008, *ANSYS-CFX, User Manual,* USA.

Technosub Inc., http://technosub.net/.

APPENDIX: NOMENCLATURE

B	source term (Nm^{-3})
b	height (m)
d	diameter (m)
e	width (m)
g	acceleration of gravity (ms^{-2})
H	head (m)
P	power (W)
p	pressure (Nm^{-2})
p_κ	turbulence production due to viscous and buoyancy forces
Q	volume flow rate (m^3s^{-1})
r	radial coordinate (m)
V	absolute velocity (ms^{-1})
v	flow velocity in y direction (ms^{-1})
U	velocity or tangential velocity (ms^{-1})
u	flow velocity in x direction (ms^{-1})
W	relative velocity (ms^{-1})
w	flow velocity in z direction (ms^{-1})
x	x-coordinate (m)
y	y-coordinate (m)
z	z-coordinate (m)

Greek symbols

α	angle between V and U (°)
β	blade angle between W and U (°)
Δ	difference
ε	turbulence dissipation ($m^2\ s^{-3}$)
η	efficiency
κ	turbulence kinetic energy ($kg\ m^{-2}\ s^{-2}$)
θ	angle (°)
ρ	fluid density ($kg\ m^{-3}$)
μ	dynamic viscosity (Pa s)
μ_{eff}	effective viscosity (Pa s)
μ_s	slip factor
μ_t	turbulence viscosity (Pa s)
ω	angular velocity ($rad\ s^{-1}$)

Subscripts

1	inlet
2	outlet
3	volute outlet
b	blade
df	disk friction
f	flow
h	hydraulic
i	inlet or ideal
imp	impeller to fluid
L	leakage
m	mechanical
o	outlet
r	radial or perpendicular to the vector U
s	shaft or slip
u	direction of vector U
v	volumetric or volute
w	wall